

Optimal design of measurement network for neutronic activity field reconstruction by data assimilation

Bertrand Bouriquet ¹ * Jean-Philippe Argaud ²
Romain Cugnart ²

June 3, 2021

Abstract

Using data assimilation framework, to merge information from model and measurement, an optimal reconstruction of the neutronic activity field can be determined for a nuclear reactor core. In this paper, we focus on solving the inverse problem of determining an optimal repartition of the measuring instruments within the core, to get the best possible results from the data assimilation reconstruction procedure. The position optimisation is realised using Simulated Annealing algorithm, based on the Metropolis-Hastings one. Moreover, in order to address the optimisation computing challenge, algebraic improvements of data assimilation have been developed and are presented here.

keyword:

Data assimilation, neutronic, activities reconstruction, nuclear in-core measurements, inverse problem, network design, simulated annealing, Metropolis-Hastings

1 Introduction

Data assimilation methodology allows to build optimal reconstruction of activity field, within a nuclear core, using information coming from both model and measurements [1, 2, 3]. The efficiency of data assimilation for physical field reconstruction has already been demonstrated in several articles in meteorology [4, 5, 6]. Demonstration of its efficiency for nuclear core activity field reconstruction was also done in recent articles such as [7, 8, 9]. The main points of data assimilation are presented in appendix B.

However, in all those applications of data assimilation, the measurement network is considered to be known. The inverse problem consists then in optimizing the location of the measuring instruments, in order to get the best possible results from the data assimilation reconstruction procedure. Unlike the meteorological domain, for which the question cannot be addressed due to the

*bertrand.bouriquet@cerfacs.fr

¹Sciences de l'Univers au CERFACS, URA CERFACS/CNRS No 1875, 42 avenue Gaspard Coriolis, F-31057 Toulouse Cedex 01 - France

²Electricité de France, 1 avenue du Général de Gaulle, F-92141 Clamart Cedex - France

great size of the problem (over 10^6 measurement locations), the issue can be addressed and resolved for the nuclear core, as only about 10^2 to 10^3 measurement locations have to be taken into account.

The chosen method to optimise the instrument location is the well known Simulated Annealing algorithm, based on a Metropolis-Hastings one [10, 11]. This algorithm was originally designed to deal with problems of statistical physics. The first version, from N. Metropolis [10], was only focused on Boltzmann equation. Then W. K. Hastings generalized it to other cases [11]. From these methods, S. Kirkpatrick proposed some improvements [12] by changing the definition of the energy, used in the algorithm to optimise position in system presenting an inner local order. Other applications of this algorithm already exist for example in nuclear incident network design since a few years [13, 14]. A brief description of the main points of Simulated Annealing is presented in appendix A.

One of the key point in the Metropolis-Hastings algorithm is the permutation of an instrumented location in the core with a non instrumented one. This can be numerically costly to redo data assimilation calculations for each case, as it includes big matrix inversions. To make those calculation feasible, we developed methods of fast calculation, that treat instrument movement as a sequence of loss and gain of instruments. This can be considered as a perturbation of the initial state, which become then rather cheap to compute. The instrument loss fast calculation was already used in [8]. The algebraic acceleration method is recalled in appendix D.

In the paper, the first section describes the general framework of the study. In a second section, the parametrisation of simulated annealing method is provided. Then the optimisation results, of simulated annealing coupled with an assimilation procedure, are shown, either starting from standard reactor instruments distribution or from a random distribution. In a next section, the synthesis of both result is done. The global conclusion on the result of instrument location optimisation using simultaneously simulated annealing and data assimilation is then given.

2 Definition of the nuclear core working framework

The experimental set up of this study is the standard configuration of a 900 MWe nuclear Pressurized Water Reactor (PWR900), and we study the neutronic activity field reconstruction. The core is filled with a total of 157 vertical nuclear fuel assemblies, among those 50 are instrumented with Mobiles Fissions Chambers (MFC) to measure the neutronic activity fields. An horizontal slice of a PWR900 core is represented on the Figure 1. The question is then to find the location of the 50 instruments within the 157 allowed positions. We don't consider here any constraint on the location of measurements, despite the fact that real constraints exists (mainly, MFC and control rods, used for safety and steering, are incompatible). It is not realistic, but, without these constraints, the optimisation problem is more similar to experimental capabilities of new instruments on latest reactors, and is far larger and difficult to solve. Solving this unconstrained optimisation problem is then a prerequisite to take into account

any constraint.

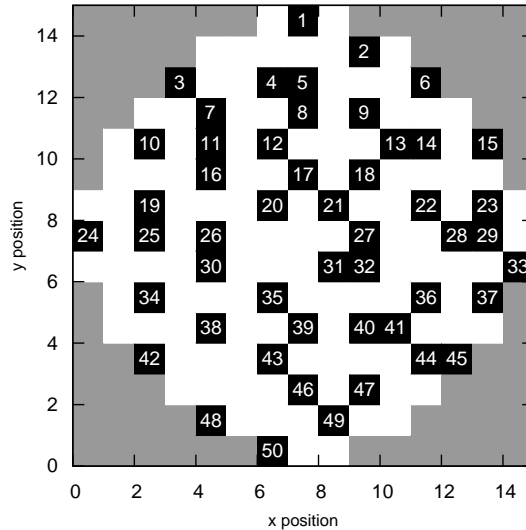


Figure 1: In the nuclear core, MFC instruments position is indicated by assemblies in black within an horizontal slice of the core. The assemblies without instrument are marked in white, and the neutronic reflector, out of the reactive core, is in grey.

To perform data assimilation, both simulation code and experimentally measured data are needed. For the simulation, the EDF newest experimental calculation code COCAGNE for nuclear cores [15, 16] is used in a standard configuration. A description of basic features of the underlying neutronic model is done in the appendix C. The physical assemblies are numerically represented using 29 vertical levels. Thus, the size of the data assimilation control vector \mathbf{x} is 4553 (157×29). The size of the observation vector \mathbf{y}^o is 1450 (50×29). All the details of data assimilation parameters, derived from those choice of model and observation space, are given in appendix C.

To have a good understanding of the instrumentation effect, we study various scenario of instrument configurations (even some that do not exist operationally and so cannot be tested experimentally). For that, synthetic data are used, that allows to have an homogeneous approach all along the document and to use twin experiment methodology. Synthetic data is generated from a model simulation, filtered through an instrument model, and noised according to a predefined measurement error density function (usually of Gaussian type).

3 Parametrisation of the simulated annealing algorithm

The global description of the well known simulated annealing and the Metropolis-Hastings algorithms is done in the appendix A. This section only focus on the specific parameters related to the problem of instrument locations optimisation,

coupled with a data assimilation procedure for the activity field reconstruction.

3.1 Definition of the energy

In the present case, the aim is not to minimise a real energy, but to improve the quality of reconstruction \mathbf{x}^a of the neutronic activity fields on the nuclear core. The reconstructed field \mathbf{x}^a is the result of a data assimilation procedure, using parameters described in appendix C, for a given instrumental configuration.

Thus we would like to minimise the distance to the true value \mathbf{x}^t of the core activity fields, that we know because we decide to set ourselves in twin experiment framework. The energy E will then be defined as the norm of the difference between the analysis \mathbf{x}^a and the true value \mathbf{x}^t , written as the following formula:

$$E(\mathbf{x}^a) = \|\mathbf{x}^a - \mathbf{x}^t\| \quad (1)$$

This definition of the energy will be used, all along the Metropolis-Hastings algorithm, for the required term in formula 7.

3.2 Measuring the evolution of the quality

To measure the evolution of the quality of an instrument configuration, as a function of the iteration in the process, a natural choice is to plot the value of the energy $E(\mathbf{x}^a)$.

However, this value has no real physical meaning. Thus, it is more interesting to study the difference of $E(\mathbf{x}^a)$ with respect to a chosen reference $E(\mathbf{x}_{ref}^a)$. This is only a shift in the energy function, but this leads to a better suited function to represent the quality of the \mathbf{x}^a reconstruction: the best is the instruments location, the closest the new quality is to zero.

We choose this reference value to be given by an analysis \mathbf{x}_{ref}^a , obtained by data assimilation, assuming each assembly in the core is instrumented with one MFC. In an idealized case, such a "limit state" can be accessed by experiment. The calculation is done with respect to the same parametrisation of data assimilation as described in the appendix C.

The quality evaluation factor q is then given by the following formula:

$$q(\mathbf{x}^a) = E(\mathbf{x}^a) - E(\mathbf{x}_{ref}^a) = \|\mathbf{x}^a - \mathbf{x}^t\| - \|\mathbf{x}_{ref}^a - \mathbf{x}^t\| \quad (2)$$

Its values are negative. Thus, if the Metropolis-Hastings algorithm improves the instrument location choices, we expect to get an increasing curve for q over the iterations.

3.3 Starting state for the optimisation algorithm

The Metropolis-Hastings algorithm is an iterative algorithm, requiring a starting point or instrument state to begin optimisation. We choose particular starting points to illustrate how is working the algorithm. Moreover, the Metropolis-Hastings algorithm is also a stochastic one. Thus assuming no seed is chosen in the random number generator, two realisations of the algorithm will lead to different sequences of evolution.

The classical PWR900 configuration is expected to be a very good one, reliable and being designed years ago. Thus, as a first possibility for the starting

point of the Metropolis-Hastings algorithm, this configuration can be chosen. This will assess the quality of this design (that originally satisfy also to a lot of operational constraints, on the contrary to the one we are seeking by optimization). In order to illustrate how is working the algorithm, two different random realisations of the algorithm will be presented based on the same initialisation in section 4.

A second possibility for the starting point is to randomly choose it. This will allow comparison of the optimal search with the one obtained with PWR900 configuration as initial point.

An another comparison can be done by using less instruments than the 50 classically considered, in order to look at the influence of the number of instruments. In this case, the starting point has to be randomly chosen, as there is no standard repartition of instruments.

3.4 Other parameters of the algorithm

As is stated in appendix A, parameters need to be chosen to run a Metropolis-Hastings algorithm. There are mainly 2 parameters to set in the present case.

The first one is the maximal number of iterations, which is the number of time that we go through the loop on instrumentation swapping. This number will be set to 1800. This value was chosen for two reasons. The first point is that we notice, through the setting up trials, that with such a number of iterations, we reach a steady state in every case we processed. As a second point, it corresponds to reasonable computing time of about 10 hours (depending on the computer used) per search and per processor.

The second parameter is the choice of the thermalisation function that fixes the evolution of the pseudo-temperature in the algorithm. We experiment several standard thermalisation formulation, and put our final choice on a classical simple inverse function of the iteration, defined as follows:

$$T_i = \frac{T_0}{i + 1} \quad (3)$$

where i is the iteration step. The initial value T_0 of the temperature was set to 0.05. With such a definition, we got satisfactory result for the optimisation algorithm.

4 Result of optimisation from PWR900 configuration

In the figure 2 and 3, two cases are presented, based on the same initialisation and on different random realization. On those figure, the red crosses represent the quality of the configuration at the current iteration, and the blue asterisks represent the quality of the best state founded since the beginning.

First, we are looking at the best state found curve. In both figures 2 and 3, it can be noticed that the algorithm reach a better state at the end than the initial one. Looking at the quality of the final state in the two cases, it can be noticed that they are very close. Looking on a set of realisation of the optimisation (not presented here), the final state is always around the same level of quality with a rather small dispersion (around 0.002, that is around

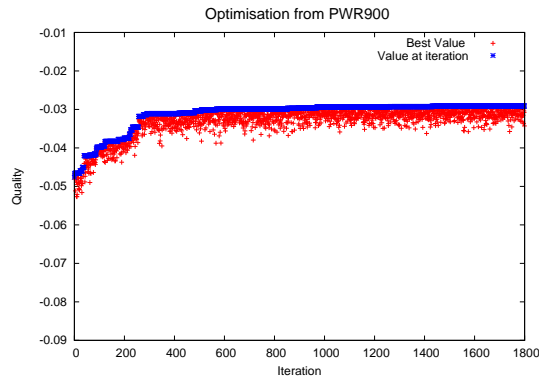


Figure 2: Evolution of the quality of the reconstruction as a function of the iteration on 1800 steps (first random realization). At each step are represented the best evaluated quality as well as the quality at the current iteration.

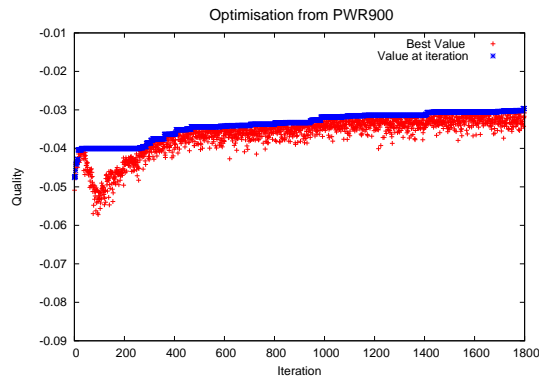


Figure 3: Evolution of the quality of the reconstruction as a function of the iteration on 1800 steps (second random realization). At each step are represented the best evaluated quality as well as the quality at the current iteration.

5%). In both cases, in a first phase, the quality of the configuration improves fairly quickly and a good configuration can be found after around 300 iterations. After that, the improvement of the configuration is very slow and even stagnate above 800 iterations.

Then, it is interesting to have a look at the value of the quality of the current state for each iteration, to better understand the behaviour of the Metropolis-Hastings algorithm. The plot of the current state in figure 2 is the typical one we got over several realisation. The current state is "oscillating" around the current best state, to find a new optimal state. The behaviour of the algorithm plotted in figure 3 is less common, but very illustrative of the potentiality of the method. We notice that the quality of the final state is about the same as the one of the figure 2. But in figure 3, we notice also that the current state can get very far away of the best state, for a very long time steps. This kind of minimum search, far from the current state, is one of the strong point of the present algorithm. This research of a new optimal state is possible because of the highest pseudo

temperature at the beginning of the process given by equation 3. The most interesting fact is that, whatever how far the method explore the state space, finally it converge again to a state of good quality. This property of Metropolis-Hastings algorithm, noticed qualitatively here, have been demonstrated rather recently mathematically as mentioned in reference [17].

At the end of the optimisation process, a new set of locations for the instruments is obtained. The set of location coming from the two previous optimisations are plotted in figures 4 and 5.

Location set represented in 4 and 5 have, at glance, no common point. However, from the point of view of the quality defined by equation 2, those two repartitions are very close. This prove not only that one optimal state does exist, but also that there is an ensemble of optimal states of rather close quality.

Examining more precisely both figure 4 and 5 (and other realisation not presented here), some common features can be discussed. In particular, there is a tendency to form small clusters of instruments, mainly localised in the centre of core. Another feature is the repartition of several individual instruments around the core. However, a detailed study over many realisations shows that such features are not significant.

5 Result of optimisation from random configuration and dependency to instruments number

Without an initial guess of the instrument repartition as the one of standard PWR900, the natural choice of a starting repartition is to take them randomly. To be in the same condition as in the PWR900 case, we choose to use 50 instruments randomly located in the core. Using random location is, at the same time, a good opportunity to get information on method and result when less instruments are available. Thus the case where only 10 instruments are in the core will be studied too.

To define the problem, a brief study of the property of the result of data assimilation quality for random instruments repartition has been done. Over a set of 1000 random distribution of the 50 instruments, it can be noticed that the quality q of all data assimilation reconstructions \mathbf{x}^a (with respect to formula 2) are distributed following as Gaussian distribution of mean $m = -0.0832$ and a standard deviation $\sigma = 0.0078$.

This already means that, with a value of $q = -0.0476$, the PWR900 standard repartition is an excellent choice, with a far greater quality.

Assuming only 10 instruments, the distribution of the quality q of the analysis \mathbf{x}^a still have Gaussian shapes but with a mean value of $m = -0.0868$ and a standard deviation of $\sigma = 0.076$. The very small difference between the mean value of both distributions proves that, due to distance of influence included in data assimilation procedure, inappropriate localisation of the instruments can result in decreasing performance of the method, as already noticed in reference [9].

Now we look at the evolution of the quality of the data assimilation reconstruction as a function of iterations of Metropolis algorithm. In the figures 6 and 7, those two cases are presented. Within those figures, as in figures 2 and 3, the

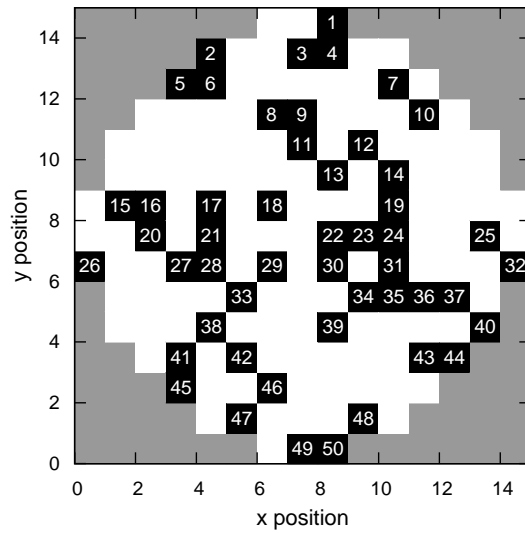


Figure 4: The optimised positions of MFC instruments after a first random realisation are localised in assemblies in black, within an horizontal slice of the core. The assemblies without instrument are marked in white and the reflector, out of the reactive core, is marked in grey.

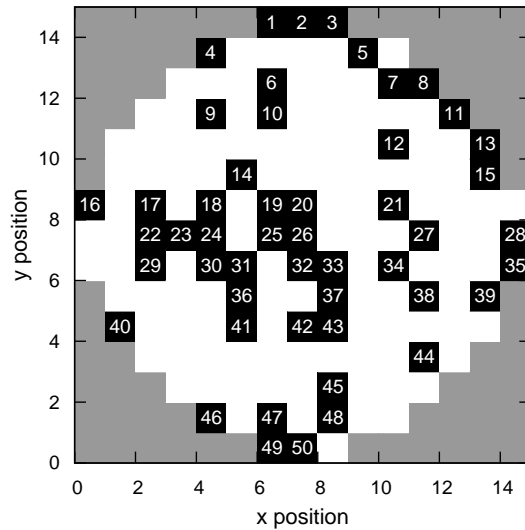


Figure 5: The optimised positions of MFC instruments after a second random realisation are localised in assemblies in black, within an horizontal slice of the core. The assemblies without instrument are marked in white and the reflector, out of the reactive core, is marked in grey.

crosses in red represent the quality of the configuration at the current iteration and the asterisks in blue represent the quality of the best state founded.

In both figures 6 and 7, it can be noticed a very fast improvement, of the

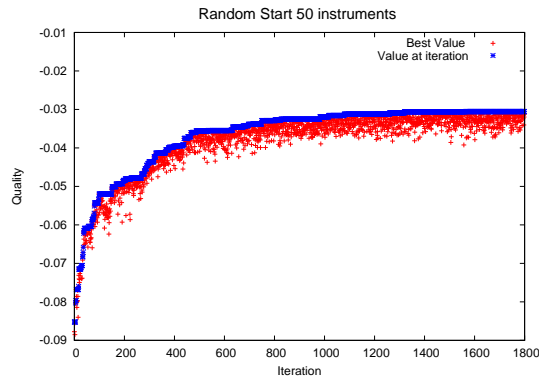


Figure 6: Evolution of the quality of the reconstruction using 50 instruments, initially randomly localized, as a function of the iteration on 1800 steps. At each step are represented the best evaluated quality, as well as the quality at the current iteration.

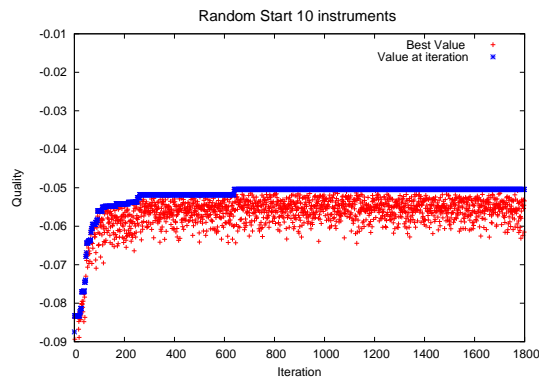


Figure 7: Evolution of the quality of the reconstruction using 10 instruments, initially randomly localized, as a function of the iteration on 1800 steps. At each step are represented the best evaluated quality, as well as the quality at the current iteration.

quality of the instruments setting, in very few iterations of the Metropolis-Hastings algorithm. This initial phase is followed by a slow evolution of the quality, and then by a stagnation phase. Stagnation phase is reached around after 600 iterations (resp. 300) for 50 (resp. 10) instruments. This difference can be easily explained, considering the space of possible configurations for 50 instruments in the core is far more large than the one of 10 instruments. The final state quality value is of -0.0305 (resp. -0.0504) for 50 (resp. 10) instruments. Those qualities after optimisation are coherent with the amount of available information, that is, of number of available instruments. This was shown in [9].

The behaviour of the current state is typical of the Metropolis-Hastings algorithm on both figures 6 and 7. It is then interesting to compare the locations of the instruments in the optimised state for both cases of 50 and 10 instruments.

Those locations are presented in figures 8 and 9.

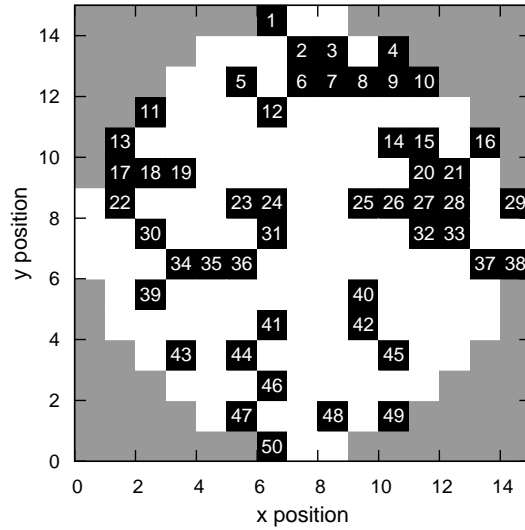


Figure 8: The optimised locations of 50 MFC instruments are localised in assemblies in black within the horizontal slice of the core. The assemblies without instrument are marked in white and the reflector, out of the reactive core, is in grey.

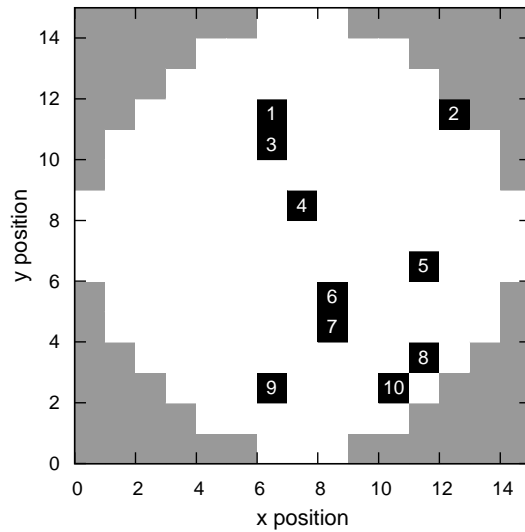


Figure 9: The optimised locations of 10 MFC instruments are localised in assemblies in black within the horizontal slice of the core. The assemblies without instrument are marked in white and the reflector, out of the reactive core, is in grey.

In both figures 8 and 9 appear the same features as the one obtained in figures 4 and 5, coming from optimisation of an initial PWR900 standard con-

figuration. Those features are a tendency to form small cluster of instruments mainly localised in the centre of core, and the repartition of several instrument around the core. However, this is still statistically irrelevant.

6 Synthesis of the results

Using the information gathered from the various uses of the method, we make a synthetic plot of the information obtained and comment it. On figure 10 are plotted the quality of the best evaluation as a function of the number of iteration coming from figures 2, 6 and 7.

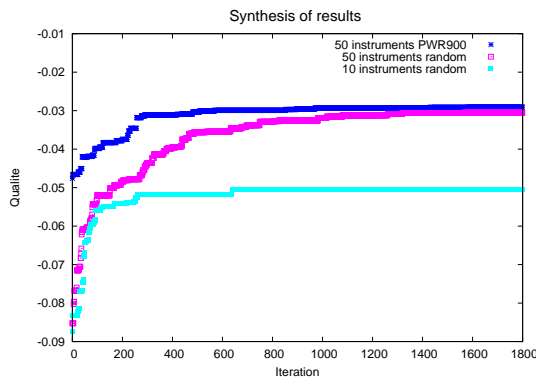


Figure 10: Evolution of the quality of reconstruction as a function of the iteration on 1800 steps, with 50 instruments initialised by PWR900 or random configurations, and with 10 instruments initialised randomly.

The first remark on figure 10 is that, whatever are the initial condition (instruments repartitions or number of instruments), the simulated annealing method allows to find a better solution.

One interesting result of this study is, as expected, the good quality of the PWR900 standard instruments distribution. Without any optimisation, the quality of this repartition is $q = -0.0476$, that should be compared to a mean value of $m = -0.0832$ for several random repartition with 50 instruments. We recall that the optimisation procedure is done without any constraints, which is not physically comparable with the PWR900 and its standard instruments distribution.

Thus, this is not a good idea to chose randomly the position of the instruments, even with a data assimilation procedure to make an optimal determination of the activity field. However, looking for the case with 50 instruments, after optimisation, the final results have the same quality with a quality factor q close to -0.0325 . This is a experimental confirmation of the theoretical result about convergence of simulated annealing method [17], this even if the final state for the same quality do not look alike as it can be seen in figures 4 and 8.

Using different number of instruments as in section 5, we notice interesting results. Observing the starting quality value q of results with data assimilation, the situation is rather blurry, as the quality with 50 instruments is close to the one with 10 instruments. Then, after position optimisation by simulated

annealing, ordering is clearly done according to the instruments number: the more instruments we use, the best quality we get. Moreover, this result is general, and final quality is always ordered respect to the number of available instruments.

All those results demonstrate the efficiency and robustness of the simulated annealing method for instruments position optimisation. This is even more stringent considering that the method is applied in link with data assimilation technique, that already enrich the global information on the whole system.

7 Conclusion

From this study, two important results are enlightened.

First, the standard PWR900 instruments repartition is characterized by an excitingly good quality. This instruments repartition is *a priori* the best we know, even if it was not originally designed using a data assimilation framework background.

The second point is that the simulated annealing method can always find a ameliorated instrument locations set. Moreover, as expected theoretically [17], the final state is of the same quality whatever is the starting point. And using a reduced number of instruments, the final organisation has always a quality that is increasing with the increase of the number of instruments.

Those results demonstrate that, within the framework of neutronic simulation for nuclear PWR, and using a reasonable size for the discrete space in which to optimize the instruments (below 10^4 points), it is possible to do instruments repartition optimisation with data assimilation method. Such a work can be done more efficiently considering an algebraic optimisation of the calculations, and become still very reasonable in computing time.

Within the framework of nuclear core neutronic simulation, several developments can be done from those results. Specially, instruments repartition can be done under constraints such as symmetry or specific position for example. Moreover, use of data assimilation open the way to obtain simulated annealing optimisation with heterogeneous available instruments.

References

- [1] D. F. Parrish, J. C. Derber, The national meteorological center's spectral statistical interpolation analysis system, *Monthly Weather Review* 120 (1992) 1747–1763.
- [2] R. Todling, S. E. Cohn, Suboptimal schemes for atmospheric data assimilation based on the kalman filter, *Monthly Weather Review* 122 (1994) 2530–2557.
- [3] K. Ide, P. Courtier, M. Ghil, A. C. Lorenc, Unified notation for data assimilation: operational, sequential and variational, *Journal of the Meteorological Society of Japan* 75 (1B) (1997) 181–189.
- [4] S. M. Uppala, *et al.*, The ERA-40 re-analysis, *Quarterly Journal of the Royal Meteorological Society* 131 (612, Part B) (2005) 2961–3012.

- [5] E. Kalnay, *et al.*, The NCEP/NCAR 40-year reanalysis project, *Bulletin of American Meteorological Society* 77 (1996) 437–471.
- [6] G. J. Huffman, *et al.*, The global precipitation climatology project (GPCP) combined precipitation dataset, *Bulletin of American Meteorological Society* 78 (1997) 5–20.
- [7] S. Massart, S. Buis, P. Erhard, G. Gacon, Use of 3DVAR and Kalman filter approaches for neutronic state and parameter estimation in nuclear reactors, *Nuclear Science and Engineering* 155 (3) (2007) 409–424.
- [8] B. Bouriquet, J.-P. Argaud, P. Erhard, S. Massart, A. Ponçot, S. Ricci, O. Thual, Differential influence of instruments in nuclear core activity evaluation by data assimilation, *Nuclear Instruments and Methods in Physics Research Section A* 626-627 (2011) 97–104.
- [9] B. Bouriquet, J.-P. Argaud, P. Erhard, S. Massart, A. Ponçot, S. Ricci, O. Thual, Robustness of nuclear core activity reconstruction by data assimilation, *Nuclear Instruments and Methods in Physics Research Section A* 629 (1) (2011) 282–287.
- [10] N. Metropolis, A. W. Rosenbluth, M. N. Rosenbluth, A. H. Teller, E. Teller, Equation of state calculation by fast computing machine, *The Journal of Chemical Physics* 21 (6) (1953) 1087–1092.
- [11] W. K. Hastings, Monte Carlo sampling methods using Markov chains and their applications, *Biometrika* 57 (1) (1970) 97–109.
- [12] S. Kirkpatrick, C. D. Gelatt, M. P. Vecchi, Optimization by simulated annealing, *Science* 220 (4598) (1983) 671–680.
- [13] R. Abida, M. Bocquet, N. Vercauteren, O. Isnard, Design of a monitoring network over france in case of a radiological accident release, *Atmospheric Environment* 42 (21) (2008) 5205–5219.
- [14] R. Abida, M. Bocquet, Targeting of observation for accidental atmospheric release monitoring, *Atmospheric Environment* 43 (40) (2009) 6312–6327.
- [15] T. Courau, M. Cometto, D. Couyras, E. Girardi, N. Schwartz, Element of validation of pin by pin calculations with the future EDF calculation scheme based on APOLLO2 and COCAGNE codes, in: 2008 International Congress on Advances in Nuclear Power Plants (ICAPP’08), Embedded International Topical Meeting at the 2008 ANS Annual Meeting, June 8-12, 2008, Anaheim, California, USA, 2008.
- [16] F. Hoareau, F. Laugier, D. Couyras, Element of validation of microscopic depletion for the future EDF calculation scheme based on APOLLO2 and COCAGNE codes, in: 2008 International Congress on Advances in Nuclear Power Plants (ICAPP’08), Embedded International Topical Meeting at the 2008 ANS Annual Meeting, June 8-12, 2008, Anaheim, California, USA, 2008.
- [17] L. Michel, Analyse semi classique d’algorithmes de type metropolis, *SMF-Gazette* 123 (2010) 16–47.

- [18] O. Talagrand, Assimilation of observations, an introduction, *Journal of the Meteorological Society of Japan* 75 (1B) (1997) 191–209.
- [19] E. Kalnay, *Atmospheric Modeling, Data Assimilation and Predictability*, Cambridge University Press, 2003.
- [20] F. Bouttier, P. Courtier, Data assimilation concepts and methods, Meteorological training course lecture series, ECMWF (March 1999).
- [21] F. Rabier, H. Järvinen, E. Kilnder, J. Mahfouf, A. Simmons, The ECMWF operational implementation of four-dimensional variational assimilation. part I: Experimental results with simplified physics, *Quarterly Journal of the Royal Meteorological Society* 126 (2000) 1143–1170.
- [22] J. J. Duderstadt, L. J. Hamilton, *Nuclear reactor analysis*, John Wiley & Sons, 1976.
- [23] G. Matheron, La théorie des variables régionalisées et ses applications, *Cahiers du Centre de Morphologie Mathématique de l'ENSMP, Fontainebleau, Fascicule 5*, 1970.
- [24] D. Marcotte, *Géologie et géostatistique minières* (2008).
- [25] F. Zhang, *The Schur complement and its applications*, Springer, 2005.

A Metropolis-Hastings algorithm

The algorithm used for position optimisation is the Metropolis-Hastings one. It was initially used to describe the thermodynamically evolution of a system, and the first algorithm was written by N. Metropolis, A. W. Rosenbluth, M. N. Rosenbluth, A. H. Teller, and E. Teller [10]. In this version, only a Boltzmann type distribution was considered as it is the main one used in statistical physics. Then, in 1970, W. K. Hastings extends this algorithm to other distributions [11].

The method is a random walk in instruments localisation space, and so an iterative algorithm. This random walk use a probability Q to chose the next possible position x , moving from x_k at step k . The transition probability is $Q(x_k, x)$. Thus the probability that the whole system go from x_k to x at step $k + 1$ (which means $x_{k+1} = x$) is then defined as follow:

$$P(x_{t+1} = x|x_t) = \min \left\{ \frac{\pi(x)Q(x_t, x)}{\pi(x_t)Q(x, x_t)}, 1 \right\} \quad (4)$$

The remaining probability is the one to stay in x_k :

$$P(x_{t+1} = x_t|x_t) = 1 - P(x_{t+1} = x|x_t). \quad (5)$$

In the very common case of symmetric evolution, which means that $Q(x, y) = Q(y, x)$, some extra simplifications can be obtained. When optimising instruments location, we are in such a case, as changing position of an instrument and then making the invert operation leads to the same first repartition. Moreover, the choice of both, the instrument to move, and its new localisation, are perfectly random:

- with a probability of 1 if $\pi(x) \geq \pi(x_t)$
- with a probability of $\frac{\pi(x)}{\pi(x_t)}$ else

using a given probability distribution π . Any kind of probability distribution can be taken into account. In the present case, like in many applications of Metropolis algorithm, a Boltzmann distribution will be used as probability function. The Boltzmann distribution is defined by the following formula:

$$\pi(x) = e^{-\frac{E(x)}{T}} \quad (6)$$

where $E(x) = E$ is an evaluation of the quality of the state (such as a physical energy or something else) of the state x , and where T is a temperature or a pseudo-temperature associated to E . Thus, in the equation 4, when we make the ratio $\frac{\pi(x)}{\pi(x_t)}$, we obtain the following formula:

$$\pi(x) = e^{-\frac{E(x)+E(x_k)}{T}} = e^{-\frac{\Delta(x, x_k)}{T}} \quad (7)$$

This is this formula used here for the Metropolis algorithm.

The final algorithm of positions optimisation is then a loop, that last until a condition on number of iteration or on energy limit is reached. Within the loop, the following actions are realised:

- Swap two instruments or displace one instrument by swapping with a void place,
- Evaluate the pseudo energy E of the new configuration,
- Compare and record the best configuration founded,
- Chose evolution of the instrument pattern according to probability law given by equation 7,
- Go back to first step.

The algorithm is finally simple and reliable. Those type of methods have been used for positions optimisation in several applications, and one of the first and most relevant result was obtained for optimisation of chip design by S. Kirkpatrick, C. D. Gelatt and M. P. Vecchi [12].

B Data assimilation

We briefly introduce the useful data assimilation key points to understand their use, as applied in [18, 19, 20].

Data assimilation is a wide domain and these techniques are, for example, the keys of the nowadays meteorological operational forecasts [21]. This is through advanced data assimilation methods that weather forecasting has been drastically improved during the last 30 years. All the available data, from satellites, aircraft or ground measurements, are used in conjunction with complex numerical weather models.

The goal of data assimilation methods is to estimate the true value \mathbf{x}^t of the state of the considered system, where the t index stands for "true". The basic idea is to combine information from an *a priori* knowledge on the state of the system (usually denoted as \mathbf{x}^b , with b for "background"), and some measurements (referenced as \mathbf{y}^o , with o for "observations"). The background is usually the result of numerical simulations, but can also be derived from any *a priori* knowledge. The result of data assimilation is called the analysis, denoted by \mathbf{x}^a , and it is an estimation of the true state \mathbf{x}^t we look for.

The control and observation spaces are not necessarily the same, and a bridge between them has to be built. This is the observation operator H , that transforms values from the space of the background to the space of observations. For data assimilation purpose, we use the linearised operator \mathbf{H} of H around the background \mathbf{x}^b . The reverse operator, converting observation increments to background increments, is given by the transpose \mathbf{H}^T operator of \mathbf{H} .

Two other ingredients are necessary. The first one is the covariance matrix \mathbf{R} of observation errors, defined as $\mathbf{R} = E[(\mathbf{y}^o - H(\mathbf{x}^t)).(\mathbf{y}^o - H(\mathbf{x}^t))^T]$, where $E[.]$ is the mathematical expectation. It is obtained from the known errors assuming unbiased measurements, which means $E[\mathbf{y}^o - H(\mathbf{x}^t)] = 0$. The second one is the covariance matrix \mathbf{B} of background errors, defined as $\mathbf{B} = E[(\mathbf{x}^b - \mathbf{x}^t).(\mathbf{x}^b - \mathbf{x}^t)^T]$. These errors on the *a priori* state are also assumed it to be unbiased. There are many ways to get this *a priori* state and background error matrices. However, those matrices are commonly obtained from the output of a model by an evaluation of accuracy, or are the result of expert knowledge.

Within this formalism, under a static assumption of state equations, the analysis \mathbf{x}^a is the Best Linear Unbiased Estimator (BLUE), and is given by the following equation:

$$\mathbf{x}^a = \mathbf{x}^b + \mathbf{K}(\mathbf{y}^o - H\mathbf{x}^b), \quad (8)$$

where \mathbf{K} is the gain matrix such as:

$$\mathbf{K} = \mathbf{B}\mathbf{H}^T(\mathbf{H}\mathbf{B}\mathbf{H}^T + \mathbf{R})^{-1}. \quad (9)$$

Moreover, we can express the analysis error covariance matrix \mathbf{A} characterising the analysis errors $\mathbf{x}^a - \mathbf{x}^t$. This matrix is derived from \mathbf{K} as:

$$\mathbf{A} = (\mathbf{I} - \mathbf{K}\mathbf{H})\mathbf{B}, \quad (10)$$

where \mathbf{I} is the identity matrix.

It is worth noting that solving Equation 8 is, if the probability distribution is Gaussian, equivalent to minimise the following function $J(\mathbf{x})$, \mathbf{x}^a being the optimal solution:

$$J(\mathbf{x}) = (\mathbf{x} - \mathbf{x}^b)^T \mathbf{B}^{-1}(\mathbf{x} - \mathbf{x}^b) + (\mathbf{y}^o - \mathbf{H}\mathbf{x})^T \mathbf{R}^{-1}(\mathbf{y}^o - \mathbf{H}\mathbf{x}). \quad (11)$$

This minimisation is known in data assimilation as 3D-Var methodology [18].

C Data assimilation implementation

C.1 Brief description of the nuclear core modelling

The aim of a neutronic code, like COCAGNE [15, 16] from EDF, is to evaluate the neutronic activity field and all associated values within the nuclear core. This field depends on the position in the core and on the neutron energy. To do such an evaluation, the population of neutrons are divided in several groups of energy. Classically, two energy groups are considered, describing the neutronic flux by $\Phi = (\Phi_1, \Phi_2)$. The material properties depend on the position in the core. The neutronic flux Φ is identified by solving two-group diffusion equations described by:

$$\begin{cases} -\text{div}(D_1 \mathbf{grad} \Phi_1) + (\Sigma_{a1} + \Sigma_r) \Phi_1 \\ \quad \quad \quad = \frac{1}{k} (\nu_1 \Sigma_{f1} \Phi_1 + \nu_2 \Sigma_{f2} \Phi_2) \\ -\text{div}(D_2 \mathbf{grad} \Phi_2) + \Sigma_{a2} \Phi_2 - \Sigma_r \Phi_1 = 0 \end{cases} \quad (12)$$

where k is the effective neutron multiplication factor, all the quantities and the derivatives (except k) depend on the position in the core, 1 and 2 are the energy group indexes, Σ_r is the scattering cross section from group 1 to group 2, and for each group, Σ_a is the absorption cross section, D is the diffusion coefficient, and $\nu \Sigma_f$ is the corrected fission cross section.

The cross sections also depend implicitly on the concentration of boron, which is a substance added in the water used for the primary circuit to control the neutronic fission reaction. This control is described through a feedback supplementary model. This model takes into account the temperature of the

materials and of the neutron moderator, given by external thermal and thermo-hydraulic models. A detailed description of the core physic and numerical solving can be found in reference [22].

The overall numerical resolution consists in searching for boron concentration such that the eigenvalue k is equal to 1, which means that the neutron production in the core is stable and self-sustaining. It is named "critical boron" concentration computation.

The activity in the core is obtained through a combination of the fluxes $\Phi = (\Phi_1, \Phi_2)$. Numerically, the activity is given on a chosen mesh of the core. Using homogeneous materials for each assembly (for example 157 in a classical EDF PWR900 reactor), and choosing a vertical mesh compatible with the core (usually 29 vertical levels), this result is an activity field of size $157 \times 29 = 4553$ that cover all the core.

C.2 The observation operator H

The observation operator H is, in the present application, a selection procedure. This procedure extracts the values corresponding to effective measurements among the values of the numerical model space. The normalisation procedure is a scaling of the value with respect to the geometry and power of the core. The entire process is linear. Then the linear operator \mathbf{H} is identical to H . Size of the operator depend directly on the number of instruments available. In a PWR900 as we treat it, the size is (1450×4553) .

C.3 The background error covariance matrix \mathbf{B}

The \mathbf{B} matrix represents the covariance between the spatial errors for the background. In order to get those, we estimate them as the product of a correlation matrix \mathbf{C} by a normalisation factor.

The correlation \mathbf{C} matrix is built using a positive function that defines the correlations between instruments with respect to a pseudo-distance in model space. Positive functions have the property (via Bochner theorem) to build a symmetric defined positive matrix when they are used as matrix generator [23, 24]. In the present case, Second Order Auto-Regressive (SOAR) function is used to prescribe the \mathbf{C} matrix. In such a function, the amount of correlation depends from the Euclidean distance between spatial points. The lengths of radial and vertical correlation (denoted as L_r and L_z respectively, and associated to the radial r coordinate and the vertical z coordinate) have different values, which means we are dealing with a global pseudo euclidean distance. The function can be expressed as follow:

$$C(r, z) = \left(1 + \frac{r}{L_r}\right) \left(1 + \frac{|z|}{L_z}\right) \exp\left(-\frac{r}{L_r} - \frac{|z|}{L_z}\right). \quad (13)$$

The matrix obtained by the above Equation 13 is a correlation matrix. It is then multiplied by a suitable variance coefficient to get a covariance matrix. This coefficient is obtained by statistical study of differences between model and measurements on real case. In our case, the size of the \mathbf{B} matrix is related to the size of model space, so it is (4553×4553) .

C.4 The observation error covariance matrix \mathbf{R}

The observation error covariance matrix \mathbf{R} is approximated by a diagonal matrix. This assumes that no significant correlation exists between the measurement errors of the measure instruments. On the diagonal, the usual modelling is to take each value as a percentage of the corresponding observation. This can be expressed as:

$$\mathbf{R}_{jj} = (\alpha(y^o)_j)^2, \quad \forall j \quad (14)$$

The parameter α is fixed according to the accuracy of the measurement and of the representative error associated to the instrument. The size of the \mathbf{R} matrix is related to the size of observation space, so it is here of (1450×1450) for a PWR900.

D Fast calculation method for data assimilation on perturbed instruments network

The direct calculation of influence of the displacement of an instrument, which is mandatory for the Metropolis algorithm, is very time consuming because of the size of the matrices. Thus, to shorten this computing time, we developed special methods to calculate the removal or the addition of an instrument as a perturbation of a known state. Thus, changing the position of an instruments in the network corresponds to remove an instrument and then to add one, or inversely. Calculating the new analysis using such approach is then substantially faster. We present in this section the two methods, for fast analysis calculation when adding or removing instrument. Both techniques are based on Schur complement [25].

D.1 Instrument removal

Within the BLUE assimilation method, the limiting factor in calculation time are the matrices inversions. In Equation 9, the costly part is the inversion of the term \mathbf{M} defined as:

$$\mathbf{M} = \mathbf{H}\mathbf{B}\mathbf{H}^T + \mathbf{R}. \quad (15)$$

In the present case, the number of terms of \mathbf{M} is around 2.10^6 , so the inversion at each step is rather time consuming when iterating for the Metropolis algorithm. Then we try to optimise the computing cost.

We noticed that the calculations are more time consuming when only few instruments are removed. In this case the \mathbf{M} matrix remains still huge.

Thus, the idea is to use the information obtained in the inversion of the full size matrix to shorten calculation, by calculating smaller size matrix. In this case, we want to calculate the new matrix as a perturbation of the original one. This is done by exploiting the Schur complement of the matrix.

We want to suppress some instruments to a given physical configuration. With respect to the Equation 9, we need to calculate a new matrix \mathbf{K}_n . The n index is standing to designate the new matrix we want to calculate. According to Equation 15, we have to determine a new matrix \mathbf{M}_n .

This matrix \mathbf{M}_n is obtained from the knowledge of the invert of the matrix \mathbf{M}_g calculated over all the instruments. The subscript g is used to designate

the reference matrix we start from, according to Equation 15, in the case of a complete initial instruments repartition.

All the components of the new matrix \mathbf{K}_n can be obtained by suppressing the lines and columns corresponding to removed instruments in \mathbf{M}_g , inverting it and then multiplying this matrix by the corresponding \mathbf{H}_n and \mathbf{B}_n . We notice that, in our case, $\mathbf{B}_n = \mathbf{B}_g$ as procedure do not affect the model space.

To make the explanation easier (and without losing generality), we assume that the suppressed instruments correspond to the lower square of \mathbf{M}_g . If it is not the case, it is always possible to reorganise the matrix in such a way.

Now we put the matrix \mathbf{M}_g under a convenient form, separating remaining measures from removed ones. Assuming the starting matrix \mathbf{M}_g is of size $m \times m$, and assuming we plan to keep p measurements and to suppress s , \mathbf{M}_g can be written in the following way:

$$\mathbf{M}_g = \begin{pmatrix} \mathbf{P}_g & \mathbf{Q}_g \\ \mathbf{R}_g & \mathbf{S}_g \end{pmatrix}, \quad (16)$$

where:

- \mathbf{P}_g contains the remaining measurements, and is a $p \times p$ matrix,
- \mathbf{S}_g contains the suppressed measurement, and is a $s \times s$ matrix,
- \mathbf{Q}_g et \mathbf{R}_g represent the dependence between remaining measured and suppressed ones. In the particular case we are dealing with, $\mathbf{Q}_g^T = \mathbf{R}_g$. However, no further use of this property is done.

With such a decomposition, we got the equality $m = p + s$. The \mathbf{P}_g matrix corresponds to the remaining instruments, thus we have the equality:

$$\mathbf{P}_g = \mathbf{M}_n, \quad (17)$$

The Equation 16 gives the decomposition required to build the Schur complement of this matrix [25]. Under the condition that \mathbf{P}_g can be inverted, the Schur complement is the following quantity:

$$\mathbf{S}_g - \mathbf{R}_g \mathbf{P}_g^{-1} \mathbf{Q}_g, \quad (18)$$

and is noted $(\mathbf{M}_g/\mathbf{P}_g)$. This notation reads as "Schur complement of \mathbf{M}_g by \mathbf{P}_g ".

Thus we look for a cheap way to calculate \mathbf{P}_g^{-1} knowing \mathbf{M}_g^{-1} . For that, we use the Banachiewicz formula [25], that gives invert of \mathbf{M}_g as a function of \mathbf{P}_g , \mathbf{Q}_g , \mathbf{R}_g , \mathbf{S}_g and $(\mathbf{M}_g/\mathbf{P}_g)$ matrices:

$$\begin{aligned} \mathbf{M}_g^{-1} &= \begin{pmatrix} \mathbf{P}_g & \mathbf{Q}_g \\ \mathbf{R}_g & \mathbf{S}_g \end{pmatrix}^{-1} \\ &= \begin{pmatrix} \mathbf{P}_g^{-1} + \mathbf{P}_g^{-1} \mathbf{Q}_g (\mathbf{M}_g/\mathbf{P}_g)^{-1} \mathbf{R}_g \mathbf{P}_g^{-1} & -\mathbf{P}_g^{-1} \mathbf{Q}_g (\mathbf{M}_g/\mathbf{P}_g)^{-1} \\ -(\mathbf{M}_g/\mathbf{P}_g)^{-1} \mathbf{R}_g \mathbf{P}_g^{-1} & (\mathbf{M}_g/\mathbf{P}_g)^{-1} \end{pmatrix} \end{aligned} \quad (19)$$

We define the 4 sub-matrices $\tilde{\mathbf{P}}_g$, $\tilde{\mathbf{Q}}_g$, $\tilde{\mathbf{R}}_g$ and $\tilde{\mathbf{S}}_g$ by:

$$\tilde{\mathbf{P}}_g = \mathbf{P}_g^{-1} + \mathbf{P}_g^{-1} \mathbf{Q}_g (\mathbf{M}_g/\mathbf{P}_g)^{-1} \mathbf{R}_g \mathbf{P}_g^{-1}, \quad (20)$$

$$\tilde{\mathbf{Q}}_g = -\mathbf{P}_g^{-1} \mathbf{Q}_g (\mathbf{M}_g/\mathbf{P}_g)^{-1}, \quad (21)$$

$$\tilde{\mathbf{R}}_g = -(\mathbf{M}_g/\mathbf{P}_g)^{-1} \mathbf{R}_g \mathbf{P}_g^{-1}, \quad (22)$$

$$\tilde{\mathbf{S}}_g = (\mathbf{M}_g/\mathbf{P}_g)^{-1}. \quad (23)$$

Rearranging those terms we get:

$$\mathbf{P}_g^{-1} = \tilde{\mathbf{P}}_g - \tilde{\mathbf{Q}}_g \tilde{\mathbf{S}}_g^{-1} \tilde{\mathbf{R}}_g. \quad (24)$$

By hypothesis, the inverse \mathbf{M}_g^{-1} of the global matrix is known, and it is possible to extract $\tilde{\mathbf{P}}_g$, $\tilde{\mathbf{Q}}_g$, $\tilde{\mathbf{R}}_g$ and $\tilde{\mathbf{S}}_g$ from the whole inverted matrix. Thus, the main cost to obtain the inverse of \mathbf{P}_g , of size $p \times p$, becomes the inversion of the matrix $\tilde{\mathbf{S}}_g$, which size is $q \times q$. If the number of measurements to suppress is smaller than the number of remaining ones, this methods gives a notable gain. As soon as the matrix $\mathbf{P}_g^{-1} = \mathbf{M}_n^{-1}$, final calculation of \mathbf{K}_n is straightforward.

D.2 Fast calculation of the gain matrix \mathbf{K} in the case of instruments gain

The next step is to calculate the required matrix in the case of instruments gain. In this case the situation is more tricky, as the dependency between the various instruments need to be taken into account, if they do exist. As previously, the technique used is based on Schur complement.

In this part, we consider a system with two instruments labelled with number 1 and 2, and characterised by observation operators \mathbf{H}_1 et \mathbf{H}_2 . We note d_1 and d_2 the size of the spaces respectively associated with \mathbf{H}_1 and \mathbf{H}_2 . The size of the data space is denoted n . The matrix \mathbf{H}_1 and \mathbf{H}_2 are of size $d_1 \times n$ and $d_2 \times n$ respectively.

The two error covariance matrices on measurement \mathbf{R}_1 and \mathbf{R}_2 are of size $d_1 \times d_1$ and $d_2 \times d_2$ respectively. Without loosing generality, the \mathbf{B} matrix can be assumed to be unique. Both operators \mathbf{H}_1 and \mathbf{H}_2 are application from the same space of data toward different observation spaces. The dimension of the observation space is n , then the size of this matrix \mathbf{B} is $n \times n$.

Starting from the formula 9 given for independent calculation of the analysis, we got :

$$\begin{cases} \mathbf{K}_1 = \mathbf{B}\mathbf{H}_1^T(\mathbf{H}_1\mathbf{B}\mathbf{H}_1^T + \mathbf{R}_1)^{-1} \\ \mathbf{K}_2 = \mathbf{B}\mathbf{H}_2^T(\mathbf{H}_2\mathbf{B}\mathbf{H}_2^T + \mathbf{R}_2)^{-1} \end{cases} \quad (25)$$

The coupled observation operator of the whole measurement system is defined by combination of the instruments 1 and 2. Thus, the complete observation operator can be written as follow:

$$\mathbf{H} = \begin{pmatrix} \mathbf{H}_1 \\ \mathbf{H}_2 \end{pmatrix} \quad (26)$$

This is completely equivalent to exchange the two observation operators \mathbf{H}_1 and \mathbf{H}_2 . The final matrix obtained is of size $(d_1 + d_2) \times n$. Looking now at the structure of the covariance error matrix \mathbf{R} , it can be written as follow:

$$\mathbf{R} = \begin{pmatrix} \mathbf{R}_1 & \mathbf{R}_{12} \\ \mathbf{R}_{12}^T & \mathbf{R}_2 \end{pmatrix} \quad (27)$$

In the above formula, the \mathbf{R}_{12} sub-matrix is the correlation error matrix between the two instruments set. This sub-matrix contains the information required to combine both assimilation. Even if we restart a data assimilation from the beginning, this information need to be added. Without any information, in

many case, it can be assumed that no correlation does exist between the errors of each set of instruments. This is equivalent to take $\mathbf{R}_{12} = 0$. However, to keep generality, we will treat the problem assuming a non zero \mathbf{R}_{12} matrix.

From that point, all the mandatory element to realise data assimilation calculation are available. The complete matrix \mathbf{K} , described in Equation 9, can be then decomposed according to the above information as follow:

$$\mathbf{K} = \mathbf{B} \begin{pmatrix} \mathbf{H}_1^T & \mathbf{H}_2^T \end{pmatrix} \times \left(\begin{pmatrix} \mathbf{R}_1 & \mathbf{R}_{12} \\ \mathbf{R}_{12}^T & \mathbf{R}_2 \end{pmatrix} + \begin{pmatrix} \mathbf{H}_1 \\ \mathbf{H}_2 \end{pmatrix} \mathbf{B} \begin{pmatrix} \mathbf{H}_1^T & \mathbf{H}_2^T \end{pmatrix} \right)^{-1} \quad (28)$$

Doing the multiplication of \mathbf{H}_1 and \mathbf{H}_2 matrix with \mathbf{B} matrix, the previous expression becomes:

$$\mathbf{K} = \mathbf{B} \begin{pmatrix} \mathbf{H}_1^T & \mathbf{H}_2^T \end{pmatrix} \times \left(\begin{pmatrix} \mathbf{R}_1 & \mathbf{R}_{12} \\ \mathbf{R}_{12}^T & \mathbf{R}_2 \end{pmatrix} + \begin{pmatrix} \mathbf{H}_1 \mathbf{B} \mathbf{H}_1^T & \mathbf{H}_1 \mathbf{B} \mathbf{H}_2^T \\ \mathbf{H}_2 \mathbf{B} \mathbf{H}_1^T & \mathbf{H}_2 \mathbf{B} \mathbf{H}_2^T \end{pmatrix} \right)^{-1} \quad (29)$$

In the term that needs to be inverted, the matrix is decomposed as a sum of diagonal element and extra diagonal ones. The diagonals terms correspond to previously known elements, and the extra diagonal ones appear due to the interdependency between variables, both in the model (with terms $\mathbf{H}_1 \mathbf{B} \mathbf{H}_2^T$ and $\mathbf{H}_2 \mathbf{B} \mathbf{H}_1^T$) and in the observation space (with term \mathbf{R}_{12}). Thus, the equation 29 can be rewritten as :

$$\mathbf{K} = \mathbf{B} \begin{pmatrix} \mathbf{H}_1^T & \mathbf{H}_2^T \end{pmatrix} \times \left(\begin{pmatrix} \mathbf{R}_1 + \mathbf{H}_1 \mathbf{B} \mathbf{H}_1^T & \mathbf{0} \\ \mathbf{0} & \mathbf{R}_2 + \mathbf{H}_2 \mathbf{B} \mathbf{H}_2^T \end{pmatrix} + \begin{pmatrix} \mathbf{0} & \mathbf{H}_1 \mathbf{B} \mathbf{H}_2^T + \mathbf{R}_{12} \\ \mathbf{H}_2 \mathbf{B} \mathbf{H}_1^T + \mathbf{R}_{12}^T & \mathbf{0} \end{pmatrix} \right)^{-1} \quad (30)$$

To simplify the notation, let:

$$\begin{aligned} \mathbf{P}_1 &= \mathbf{H}_1 \mathbf{B} \mathbf{H}_1^T + \mathbf{R}_1 \\ \mathbf{P}_2 &= \mathbf{H}_2 \mathbf{B} \mathbf{H}_2^T + \mathbf{R}_2 \end{aligned} \quad (31)$$

and:

$$\mathbf{P} = \begin{pmatrix} \mathbf{P}_1 & \mathbf{0} \\ \mathbf{0} & \mathbf{P}_2 \end{pmatrix} \quad (32)$$

If, as assumed, the data assimilation procedure for each of the instruments has already been done, the terms \mathbf{P}_1 and \mathbf{P}_2 are available as well are their inverse. Thus only extra diagonal term given by the following equation need to be treated:

$$\begin{pmatrix} \mathbf{0} & \mathbf{H}_1 \mathbf{B} \mathbf{H}_2^T + \mathbf{R}_{12} \\ \mathbf{H}_2 \mathbf{B} \mathbf{H}_1^T + \mathbf{R}_{12}^T & \mathbf{0} \end{pmatrix} \quad (33)$$

Also to simplify the notation, we denote:

$$\mathbf{S} = \mathbf{H}_1 \mathbf{B} \mathbf{H}_2^T + \mathbf{R}_{12} \quad (34)$$

The other term of the matrix of Equation 33 can then be obtained by transposing the previous \mathbf{S} matrix:

$$\mathbf{S}^T = \mathbf{H}_2 \mathbf{B} \mathbf{H}_1^T + \mathbf{R}_{12}^T \quad (35)$$

It worth to recall that \mathbf{B} is a symmetric positive defined matrix, thus the equality $\mathbf{B}^T = \mathbf{B}$ can be used.

Now, the aim is to put the part to invert in equation 30 under a specific form, that will ease the inversion. In this purpose, we write:

$$\mathbf{U} = \begin{pmatrix} \mathbf{0} & \mathbf{S} \\ \mathbf{I} & \mathbf{0} \end{pmatrix} \quad (36)$$

and:

$$\mathbf{V} = \begin{pmatrix} \mathbf{S}^T & \mathbf{0} \\ \mathbf{0} & \mathbf{I} \end{pmatrix} \quad (37)$$

If both matrix are multiplied in the following way, we notice a very useful property:

$$\mathbf{UV} = \begin{pmatrix} \mathbf{0} & \mathbf{S} \\ \mathbf{S}^T & \mathbf{0} \end{pmatrix} \quad (38)$$

In equation 38, we notice that extra diagonal terms can be expressed as a product of two matrix. Thus, rewriting the inverted term in equation 30, we have to calculate the following:

$$(\mathbf{P} + \mathbf{UV})^{-1} \quad (39)$$

This is from that expression that we realise inversion through Woodbury formula [25] written below:

$$(\mathbf{P} - \mathbf{QR})^{-1} = \mathbf{P}^{-1} + \mathbf{P}^{-1}\mathbf{Q}(\mathbf{I} - \mathbf{RP}^{-1}\mathbf{Q})^{-1}\mathbf{RP}^{-1} \quad (40)$$

Changing sign on the left side, we obtain:

$$(\mathbf{P} + \mathbf{QR})^{-1} = \mathbf{P}^{-1} - \mathbf{P}^{-1}\mathbf{Q}(\mathbf{I} + \mathbf{RP}^{-1}\mathbf{Q})^{-1}\mathbf{RP}^{-1} \quad (41)$$

From equation 41, we calculate the inversion needed in formula 39. First, we look after term \mathbf{P} in equation 39. The \mathbf{P} matrix is block-diagonal, thus we got :

$$\mathbf{P}^{-1} = \begin{pmatrix} \mathbf{P}_1^{-1} & \mathbf{0} \\ \mathbf{0} & \mathbf{P}_2^{-1} \end{pmatrix} \quad (42)$$

Terms of the matrix are supposed to be known and stored *a priori*. Thus respect to formula 41, we got :

$$(\mathbf{P} + \mathbf{UV})^{-1} = \mathbf{P}^{-1} - \mathbf{P}^{-1}\mathbf{U}(\mathbf{I} + \mathbf{VP}^{-1}\mathbf{U})^{-1}\mathbf{VP}^{-1} \quad (43)$$

We take the following notation:

$$\mathbf{C} = \mathbf{P}^{-1}\mathbf{U}(\mathbf{I} + \mathbf{VP}^{-1}\mathbf{U})^{-1}\mathbf{VP}^{-1} \quad (44)$$

Thus a new formulation of that gain matrix \mathbf{K} is obtained:

$$\mathbf{K} = \mathbf{BH}(\mathbf{P}^{-1} - \mathbf{C}) \quad (45)$$

Within this equation, the term \mathbf{BHP}^{-1} corresponds to join together the column of both matrix \mathbf{K}_1 and \mathbf{K}_2 from equation 25, that are respectively of size $n \times d_1$ and $n \times d_2$. We will denote \mathbf{K}_0 this term \mathbf{BHP}^{-1} , and thus we got:

$$\mathbf{K}_0 = \begin{pmatrix} \mathbf{K}_1 & \mathbf{K}_2 \end{pmatrix} = \mathbf{BHP}^{-1} \quad (46)$$

In the above equation, the 0 index notice that the gain matrix is build on the basis of the matrix of each instruments set independently. Thus we can rewrite equation 45 in the following way :

$$\mathbf{K} = \mathbf{K}_0 - \mathbf{BHC} \quad (47)$$

The term \mathbf{BHC} in equation 47 can be then interpreted as a correction to the matrix \mathbf{K}_0 , that is the simple coupling of the two original \mathbf{K} matrix. Thus, we have build here a inversion method, where we can dissociate the contributions of each instrument and the one coming from their joint use.

Looking more in detail to the matrix \mathbf{C} , defined by equation 44, some points can be noticed. In the term $(\mathbf{I} - \mathbf{VP}^{-1}\mathbf{U})^{-1}$ to be inverted, we recall that \mathbf{P}^{-1} matrix is of size $(d_1 + d_2) \times (d_1 + d_2)$. The \mathbf{V} and \mathbf{U} matrices are respectively of size $2d_2 \times (d_1 + d_2)$ and $(d_1 + d_2) \times 2d_2$. The matrix that need do be inverted in equation 44 is then of size $2d_2 \times 2d_2$. If the size of the observation space associated to instrument 2 is smaller that the size of the observation space of instrument 1, it is far better to use this method. Of course the instrument denoted 1 and 2 can be ordered in such a way that $d_1 > d_2$, which ensure that the method always gives benefits.

In the case of the permutation of instrument, we only know the analysis of the intermediate matrix for the all the instrument but one. Then the calculation of the analysis for only one instrument need to be performed before using this method. This correspond on overall to the inversion of an extra d_2 size matrix, which is rather cheap in calculation time.